I&EC research
Industrial & Engineering Chemistry Research
pubs.acs.org/IECR
Article

Mathematical Model for a Three-Phase Enzymatic Reaction System

Siyu Zou, Dandan Wang, Jie Xiao,* and Xinjian Feng*

Cite This: *Ind. Eng. Chem. Res.* 2023, 62, 4337−4343
Read Online
ACCESS | Metrics & More | Article Recommendations | Supporting Information

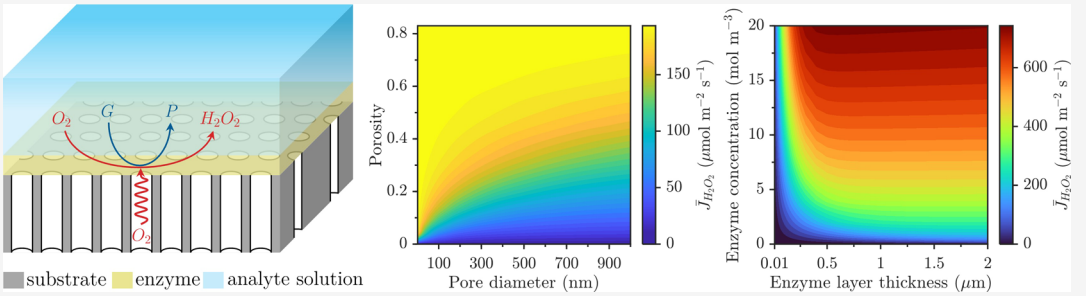

ABSTRACT: The enzymatic reaction system with a solid−liquid−gas three-phase interface microenvironment allows oxygen to be directly supplied to the oxidase catalytic reaction from the gas phase, effectively improving enzyme kinetics as compared with the conventional two-phase system. For this new system, a mathematical model is developed in this work to describe the enzymatic reaction coupled with interphase mass transfer, by which the influences of three-phase interfacial microenvironment on reaction kinetics can be systematically and quantitatively explored. The numerical simulations reveal that the flux of oxygen transport across the interface between the gas phase and the enzyme layer dominantly determines the H_2O_2 production rate. The porous substrate possessing larger porosity and smaller pores, when coated with a thick and concentrated enzyme layer, can potentially lead to higher oxygen supply and hence a higher H_2O_2 production rate. Moreover, regardless of the pore diameter, the H_2O_2 production rate remains constant after the porosity is greater than 0.8, and if the enzyme concentration is not less than 5 mol m^{-3}, the H_2O_2 production rate no longer changes after the thickness of the enzyme layer is greater than 0.5 μm. This work offers a powerful in silico tool for the investigation of the three-phase enzymatic reaction system. The quantitative results and mechanistic findings will lead to optimized design of this promising system.

INTRODUCTION

The oxidase enzymatic reactions are widely used in energy conversion,[1,2] health monitoring,[3,4] and other fields.[5−7] The development of a high-performance oxidase enzymatic reaction system has emerged as a critical area of study. Generally, the oxidase enzymatic reactions occur in a traditional solid−liquid two-phase interface, where the required oxygen is supplied from the liquid phase. The low solubility and the slow mass transfer rate of oxygen in the liquid phase limit the enzymatic reaction kinetics. Recently, this limitation has been addressed by introducing the solid−liquid−gas three-phase interface microenvironment into the oxidase enzymatic reaction systems.[8,9] A porous hydrophobic substrate is crucial in the system. When the hydrophobic substrate contacts an electrolyte, the gas transport channel is formed inside the porous structure, leading to the formation of the solid−liquid−gas three-phase interfacial microenvironment.[10−13] This allows the oxygen to be rapidly supplied from the adjacent gas phase rather than the liquid phase.

Existing efforts demonstrate that the introduction of a three-phase interface can indeed enhance the enzymatic reaction kinetics up to tens of times.[14−16] It was found that the system performance depends heavily on the three-phase interfacial microenvironment reflected by four key parameters, i.e., the structural parameters of the porous substrate: the porosity ϵ, the pore diameter d_{pore}, and the parameters of the enzyme layer: the thickness of the enzyme layer δ_{EL} and the enzyme concentration $[E_T]$. However, disclosing the underlying mechanisms remains a challenging task due to the intricate intercorrelations between these parameters and reaction kinetics.

Mathematical modeling is an effective and promising method for the investigation of transport phenomena[17,18] and reaction kinetics.[19−25] In this work, we report a novel mathematical model for a three-phase oxidase enzymatic reaction system based on glucose oxidase (GOx), a model enzyme. A steady-state isothermal 2D model was developed to describe interphase (gas dissolution) and intraphase (species

Received: December 13, 2022
Revised: February 22, 2023
Accepted: February 22, 2023
Published: March 2, 2023

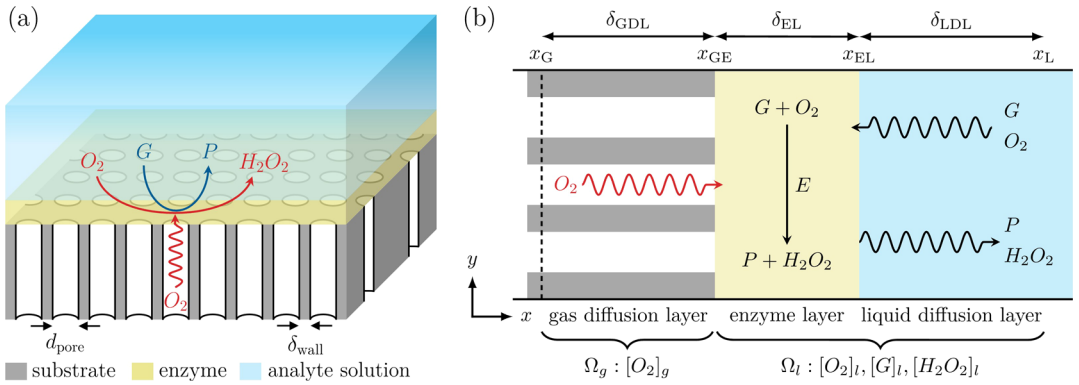

Figure 1. Schematic diagram of the three-phase enzymatic reaction system based on the glucose oxidase (GOx). (a) Components of the three-phase oxidase enzymatic reaction system, the structural parameters of the porous substrate (d_{pore} is the pore diameter, and δ_{wall} is the thickness of pore wall). (b) Computational domains, dimensions, enzymatic reaction, and main physical quantities in the model.

diffusion) mass transfer and enzyme catalysis reaction. For optimized design of oxidase enzymatic reaction systems, numerical simulations were carried out to understand these critical processes. The mathematical model can help to explain how the parameters of the three-phase interfacial microenvironment affect transport phenomena and reaction kinetics within the three-phase oxidase enzymatic reaction system by carrying out systematically designed in silico experiments. This model is expected to be an efficient tool to improve the performance of oxidase enzymatic reaction systems.

MODEL DEVELOPMENT

System Description and Model Assumptions. The three-phase oxidase enzymatic reaction system consists of a porous hydrophobic substrate with nanochannel arrays, an enzyme layer, and an analyte solution. As shown in Figure 1a, the GOx was immobilized on the surface of the substrate by drop-casting to form an enzyme layer. The enzyme layer is completely wetted by the liquid phase, and it is a two-phase layer containing solid and liquid phases. However, the hydrophobic substrate cannot be wetted and hence forms gas transport channels inside. The solid phase (the enzyme layer covered on the hydrophobic substrate), liquid phase (the analyte solution in the enzyme layer), and gas phase (the air in the pores of the hydrophobic substrate) hence coexist and form the three-phase microenvironment. The high-concentration oxygen in the gas phase could be rapidly transported to the enzyme layer through the three-phase interface.

In the three-phase enzymatic reaction system, the oxygen dissolution occurs at the solid−liquid−gas three-phase interface. The enzyme catalysis reaction occurs in the enzyme layer. Three species including glucose, oxygen, and hydrogen peroxide (H_2O_2) participate in the enzyme catalysis reaction. Glucose and oxygen diffuse into the enzyme layer and react with GOx to produce H_2O_2 in situ. Then, the H_2O_2 diffuses out of the enzyme layer, which is related to the concentration of the analyte.

A schematic diagram of the model is shown in Figure 1b. All 2D and 3D simulations were carried out on one node of a high-performance computing cluster, which has the Intel Xeon (R) Silver 4214R CPU (2.40 GHz and 48 cores) and 128 GB memory. In the case of d_{pore} = 100 nm, ϵ = 0.4, δ_{EL} = 1 μm, and $[E_T]$ = 1 mol m^{-3}, the computational time for the 2D and 3D models are about 11 and 493 s, respectively. There is about a 45-fold difference in computational time between the 2D and 3D models. One should note that there are thousands of cases to be simulated in our parametric studies. Considering the need for a large number of in silico experiments, the computational demand for the 3D model is too high. Hence, main mass transport and concentration gradient are only considered in the x and y directions and the 2D model is used. Dilute species theory[23] is used for gas-phase species and liquid-phase species, and hence, Fick's law[26] is used to describe mass transport. The diffusion coefficients of all species remain constant. The model is constructed by three separated computational domains, including the gas diffusion layer (GDL) formed by the porous substrate, the enzyme layer (EL), and the liquid diffusion layer (LDL) formed by the analyte solution. x and y axes represent directions that are parallel and perpendicular to the pore in GDL, respectively. Two diffusion layers (GDL and LDL) describe the diffusion resistance of each species before it reaches the EL surface.[22] The thickness of the diffusion layer is the same for each species and remains unchanged with time. The diffusion layer should be taken into consideration in the model when the EL thickness (δ_{EL}) is thinner than about 25 times of LDL thickness (δ_{LDL}) or GDL thickness (δ_{GDL}) to reduce the prediction deviation of the model.[22] The GDL is modeled as the gas physical field (Ω_g). The EL and LDL are modeled as the liquid physical field (Ω_l). The oxygen in the gas phase needs to be dissolved in the liquid phase before it can participate in the enzyme catalysis reactions. The interphase transport phenomena between Ω_g and Ω_l are coupled using specific boundary conditions. The mass transport phenomena in three layers are described by the isothermal reaction-diffusion equations. The enzymatic reactions are modeled by ping-pong mechanisms. The modeling methods and experimental validations are detailed in the Supporting Information.

Mass Transport in the Gas Diffusion Layer. In the GDL, the oxygen diffusion in the porous substrate and the oxygen dissolution at the three-phase interface are considered. The air is treated as diluted species, which can be described by Fick's diffusion law. The general form of the governing equation in the GDL can be written as follows

$$-D_{GDL,i}\nabla^2[i]_g = 0 \quad (1)$$

where $D_{GDL,i}$ is the effective diffusion coefficient of species i in the GDL and m2 s^{-1}; $[i]_g$ is the concentration of species i in the Ω_g (i.e., GDL), mol m^{-3}. The symbol i in the GDL only

https://doi.org/10.1021/acs.iecr.2c04492
Ind. Eng. Chem. Res. 2023, 62, 4337−4343

denotes oxygen since only oxygen is involved in the enzyme catalysis reaction in the gas phase.

When the diffusion of gas molecules occurs in pores, the gas flux is possibly reduced by the collisions between gas molecules and walls.[26] If the pore diameter is much smaller than the mean free path of the gas molecules, the collisions will occur more frequently between molecules and walls rather than between molecules. This diffusion mechanism is known as the Knudsen diffusion.[26] In larger pores, the probability of collisions between molecules and collisions between molecules and walls are comparable. The diffusion mechanism is dominated by both the Knudsen diffusion and molecular diffusion. Until the pore diameter is large enough, the molecular collisions dominate, and the diffusion mechanism reverts to pure molecular diffusion. In current studies, the pore diameter is in the range of 2−1000 nm. The Knudsen number (which is defined as $Kn = \lambda/L$, where λ is the mean free path of oxygen, at 20 °C and 1 atm, $\lambda \approx 75.1$ nm; L is the representative physical length scale, it is equal to the pore diameter in current studies) is in the range of 0.0751−37.55. In this range, the diffusion is transited from the Knudsen diffusion to the molecular diffusion. Hence, the effective diffusion coefficient of oxygen ($D_{\mathrm{GDL,O_2}}$) in pores of GDL for diluted species is calculated via the Wilke−Bosanquet model[27]

$$\frac{1}{D_{\mathrm{GDL,O_2}}} = \frac{1}{D_{\mathrm{O_2}}} + \frac{1}{D_{Kn,\mathrm{O_2}}} \tag{2}$$

where $D_{\mathrm{O_2}}$ is the molecular diffusion coefficient of oxygen in the free environment, $m^2\ s^{-1}$, it is calculated by empirical correlation;[28] $D_{Kn,\mathrm{O_2}}$ is the Knudsen diffusion coefficient of oxygen in the pore, $m^2\ s^{-1}$, it can be calculated based on the kinetics theory[28]

$$D_{Kn,\mathrm{O_2}} = \frac{d_{\mathrm{pore}}}{3}\sqrt{\frac{8R_{\mathrm{const}}T}{\pi M_{\mathrm{O_2}}}} \tag{3}$$

where d_{pore} is the pore diameter, m; R_{const} is the ideal gas constant, J mol^{-1} K^{-1}; T is system temperature, K; and $M_{\mathrm{O_2}}$ is the molecular weight of oxygen, kg mol^{-1}.

Mass Transport and Enzyme Catalysis Reaction in the Enzyme Layer. Mass transfer in the EL is coupled with reaction. It is described by Fick's diffusion law integrated with a source term for enzyme catalysis reaction.

$$-D_{\mathrm{EL},i}\nabla^2[i]_{\mathrm{l}} = R_i \tag{4}$$

where $D_{\mathrm{EL},i}$ is the diffusion coefficient of species i in the EL, $m^2\ s^{-1}$; $[i]_{\mathrm{l}}$ is the concentration of species i in the Ω_{l} (including EL), mol m^{-3}; and R_i is the reaction source term, mol $m^{-3}\ s^{-1}$; The symbol i in the EL denotes three species: glucose, oxygen, and H_2O_2.

The kinetics of GOx is modeled as a ping-pong mechanism,[29−31] which consists of two sequential reaction steps. The first reaction is the catalysis oxidation of glucose, which consumes the oxidized form of GOx and produces the reduced form of GOx at the same time. The second reaction consumes the reduced form of GOx and oxygen to yield the oxidized form of GOx and H_2O_2. The overall ping-pong reaction mechanism is shown below

$$\mathrm{E_O} + \mathrm{G} \xrightarrow{k_1} \mathrm{E_RP} \xrightarrow{k_2} \mathrm{E_R} + \mathrm{P} \tag{5}$$

$$\mathrm{E_R} + \mathrm{O_2} \xrightarrow{k_3} \mathrm{E_O(H_2O_2)} \xrightarrow{k_4} \mathrm{E_O} + \mathrm{H_2O_2} \tag{6}$$

where E_O is the oxidized form of GOx; E_R is the reduced form of GOx; G is glucose; P is the byproduct glucono-δ-lactone; E_RP and $E_O(H_2O_2)$ are two enzyme−product complexes; and k_1, k_2, k_3, and k_4 are kinetics constants. The substrate or product inhibition reaction has not been considered.

The experimental environment is isothermal. The enzyme catalysis reaction reaches steady-state rapidly. At the steady-state, the consumption rate of glucose or oxygen is equal to the generation rate of H_2O_2. The kinetics equation can be simplified. The reaction source term of the ping-pong kinetics mechanism can be expressed as follows[19]

$$R_i = \pm\frac{\alpha[E_{\mathrm{T}}]}{\frac{\beta_{\mathrm{G}}}{[\mathrm{G}]_{\mathrm{l}}} + \frac{\beta_{\mathrm{O_2}}}{[\mathrm{O_2}]_{\mathrm{l}}} + 1} \tag{7}$$

where $\alpha = k_2k_4/(k_2 + k_4)$; $\beta_{\mathrm{G}} = k_2k_4/(k_1(k_2 + k_4))$; $\beta_{\mathrm{O_2}} = (k_2k_4)/(k_3(k_2 + k_4))$; $[E_{\mathrm{T}}]$ is the total concentration of the active enzyme, mol m^{-3}; $[G]_{\mathrm{l}}$ is the glucose concentration in Ω_{l}; $[O_2]_{\mathrm{l}}$ is the oxygen concentration in Ω_{l}. It is assumed that the GOx is homogeneously distributed in the enzyme layer and $[E_{\mathrm{T}}]$ remains constant. The reactive activation of immobilized GOx is assumed to be the same as that for the soluble GOx, which has been adopted by many studies.[32] The kinetics constants provided by Atkinson and Lester[30,31] are used. The positive value of the R_i term represents the generation rate of H_2O_2, and the negative value represents the consumption rate of glucose or oxygen.

Mass Transport in the Liquid Diffusion Layer. Mass transport in the LDL is a pure diffusion process; it is also described by Fick's diffusion law. The physical quantities in the governing equation of LDL are the same as those for EL because they all belong to Ω_{l}. But the diffusion coefficients of each species in LDL are different from those in EL because the diffusion medium is different. The general form of the governing equation in the LDL can be written as follows

$$-D_{\mathrm{LDL},i}\nabla^2[i]_{\mathrm{l}} = 0 \tag{8}$$

where $D_{\mathrm{LDL},i}$ is the diffusion coefficient of species i in the LDL, $m^2\ s^{-1}$. $[i]_{\mathrm{l}}$ is the concentration of species i in the Ω_{l} (including LDL), mol m^{-3}; The symbol i in LDL denotes three species: glucose, oxygen, and H_2O_2.

All model parameters are listed in Table S1. The boundary conditions, initial conditions, model implementation, and model validation can be found in the Supporting Information.

RESULTS AND DISCUSSION

There are four main phenomena within the three-phase interface microenvironment, which are the diffusion process of oxygen within the porous substrate, the dissolution process of oxygen from the gas phase into the enzyme layer, and the mass transfer process of each species and the enzymatic catalysis reaction process within the enzyme layer.

These phenomena are mainly influenced by two groups of parameters, namely, substrate parameters (pore diameter and porosity) and enzyme layer parameters (EL thickness and enzyme concentration). The coupling effect of four types of phenomena ultimately affects the performance of three-phase enzymatic systems. This work first investigated the effect of the substrate structure on the H_2O_2 production rate. Subsequently,

https://doi.org/10.1021/acs.iecr.2c04492
Ind. Eng. Chem. Res. 2023, 62, 4337−4343

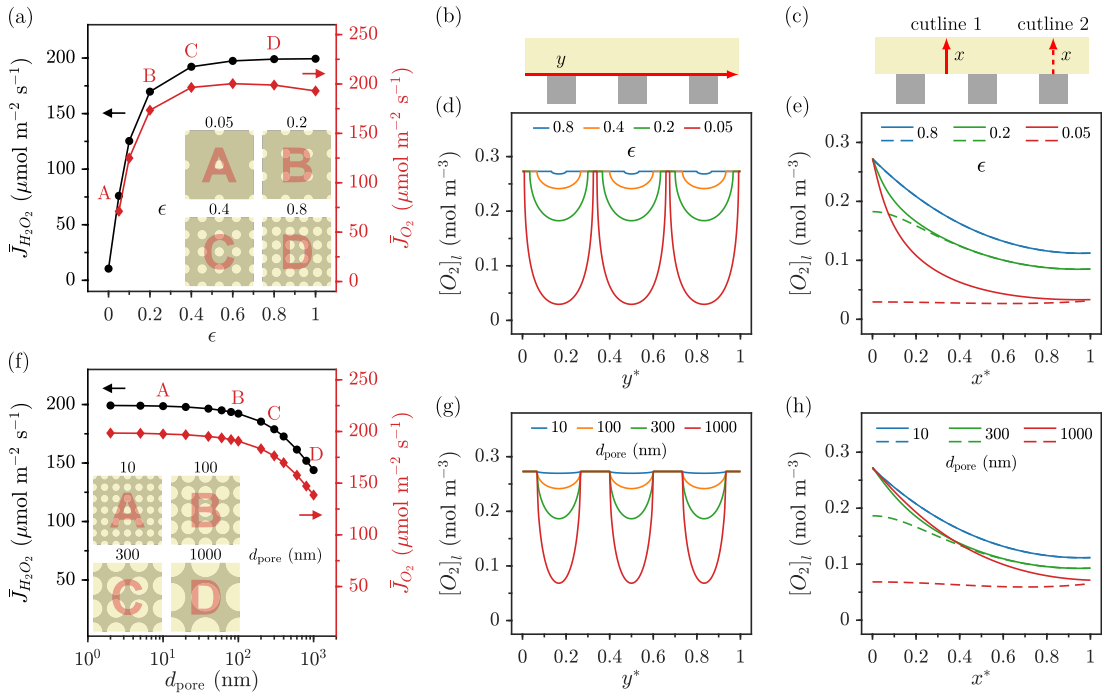

Figure 2. Effect of porosity and pore diameter on the three-phase enzymatic reaction system. (a) H_2O_2 production rate ($\bar{J}_{H_2O_2}$) and oxygen supply rate ($\bar{J}_{O_2}$) with different porosities; the inset shows the top view of the substrate with different porosities. (b,c) Schematic diagrams of a cutline at the three-phase interface and two cutlines inside the EL. (d) Oxygen concentration ($[O_2]_l$) distribution at the three-phase interface with different porosities. (e) $[O_2]_l$ distribution along two cutlines inside the EL with different porosities. (f) $\bar{J}_{H_2O_2}$ and $\bar{J}_{O_2}$ with different pore diameters; the inset shows the top view of the substrate with different pore diameters. (g) $[O_2]_l$ distribution at the three-phase interface with different pore diameters. (h) $[O_2]_l$ distribution along two cutlines inside the EL with different pore diameters.

the effect of enzyme layer parameters on the H_2O_2 production rate was investigated with a fixed substrate structure.

Effect of the Porosity of Substrate. Figure 2a shows the effect of the porosity of the substrate on the H_2O_2 production rate. The porosities range from 0 to 1. The other parameters are d_{pore} = 100 nm, $[E_T]$ = 1 mol m^{-3}, and δ_{EL} = 1 μm, where ϵ = 0 denotes the case of the diphase system and ϵ = 1 denotes that the gas phase is completely in contact with the analyte (this is not possible, but it demonstrates the limits of the system's performance). The other value of ϵ denotes the case of the three-phase system. It can be observed that increasing porosity leads to an increase in the H_2O_2 production rate. However, the growth rate of H_2O_2 production rate gradually slows down as porosity increases, and the H_2O_2 production rate eventually tends to a limit (i.e., the H_2O_2 production rate at ϵ = 1). It implies that even if ϵ < 1, the system can achieve a performance of ϵ = 1 (this is the theoretical maximum performance of the system).

It is important to note that glucose was in complete excess in all cases in the current study and would hardly limit the kinetics of the enzymatic reaction. To better understand this trend, the oxygen concentration distributions along three cutlines in the EL are analyzed (the oxygen concentration distributions in the GDL, EL, and LDL are shown in Figure S3). As shown in Figure 2b, the cutline at the three-phase interface is defined in the EL and oriented in the y direction. As shown in Figure 2c, the two cutlines in the EL are perpendicular to the EL and oriented in the x direction. The starting point of cutline 1 is the center of the pore, and the starting point of cutline 2 is the center of the pore wall. To make it easier to compare different cases, the oxygen concentration distribution along the cutlines is plotted in normalized coordinate ($x^* = \frac{x}{\delta_{EL}}$, $y^* = \frac{y}{3(d_{pore} + \delta_{wall})}$).

It is worth noting that the EL near the pore wall (e.g., the EL at cutline 2 in Figure 2c) cannot directly obtain oxygen from the gas phase. The oxygen in the gas phase primarily diffuses through the EL near the pore (e.g., the EL at cutline 1 in Figure 2c) to the EL near the pore wall. The diffusion path is at least half the thickness of the pore wall (δ_{wall}, see Figure 1a), i.e., $\delta_{wall}/2$. Because pore diameter remains constant, higher porosity means a thinner pore wall, thus the shorter the diffusion distance required for oxygen to diffuse to the EL near the pore wall from the gas phase. Consequently, the EL near the pore wall can obtain oxygen faster and avoid hypoxia.

Figure 2d shows the effect of porosity on the oxygen concentration distribution at the three-phase interface. For different porosity cases, there is a considerable fluctuation of oxygen concentration. The mean oxygen concentration can reach a higher level as porosity increases (the cases ϵ = 0.2, 0.4, and 0.8 are 1.46, 1.62, and 1.68 times higher than the case ϵ = 0.05, respectively), and the distribution of the oxygen concentration becomes more uniform. Meanwhile, higher porosity means a thinner pore wall (in the case of ϵ = 0.05, 0.2, 0.4, and 0.8, δ_{wall} = 1900, 400, 150, and 25 nm). This results in faster access to oxygen for the EL near the pore wall. As shown in Figure 2a, the higher the porosity, the greater the oxygen supply rate. This again confirms that the higher the porosity, the easier the system is to obtain oxygen and, as a result, the higher H_2O_2 production rate. Also, it should be noted that even in the presence of a porous structure impeding

https://doi.org/10.1021/acs.iecr.2c04492
Ind. Eng. Chem. Res. 2023, 62, 4337−4343

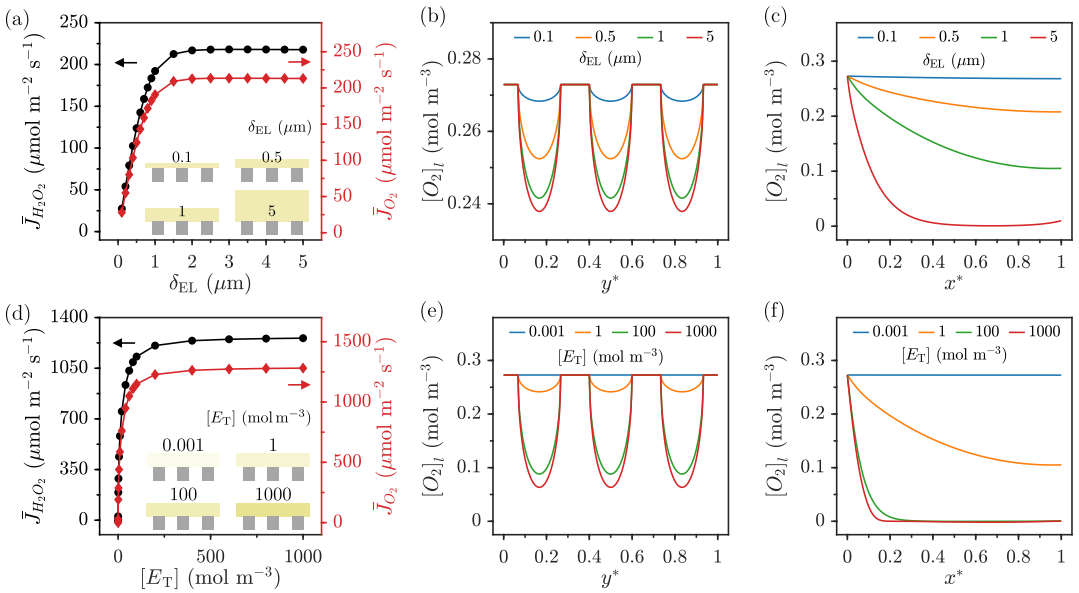

Figure 3. Effect of EL thickness and enzyme concentration on the three-phase enzymatic reaction system. (a) $\bar{J}_{H_2O_2}$ and $\bar{J}_{O_2}$ with different EL thicknesses; the inset shows the side view of the EL with different thicknesses. (b) Oxygen concentration ($[O_2]_l$) distribution at the three-phase interface with different EL thicknesses. (c) $[O_2]_l$ distribution along cutline 1 inside the EL with different EL thicknesses. (d) $\bar{J}_{H_2O_2}$ and $\bar{J}_{O_2}$ at different enzyme concentrations; the inset shows the different enzyme concentrations in color. (e) $[O_2]_l$ distribution at the three-phase interface with different enzyme concentrations. (f) $[O_2]_l$ distribution along cutline 1 inside the EL with different enzyme concentrations.

the mass transfer in the gas phase (e.g., ϵ = 0.8), the oxygen supply rate from the gas phase can be comparable to that when the gas phase is completely in contact with the liquid phase (ϵ = 1) as long as porosity reaches a certain value.

Figure 2e shows the effect of porosity on the oxygen concentration distribution along with two cutlines in the EL. The difference in oxygen concentration between the two cutlines decreases as porosity increases, implying that oxygen concentration in the y direction becomes more uniform. When ϵ > 0.8, the oxygen concentration distribution between the two cutlines differs only slightly. This also implies that the higher the porosity, the EL near the pore wall can obtain oxygen faster, resulting in a higher H_2O_2 production rate.

Effect of the Pore Diameter of Substrate. Figure 2f shows the effect of the pore diameter of the substrate on the H_2O_2 production rate. The pore diameters range from 2 to 1000 nm. The other parameters are ϵ = 0.4, $[E_T]$ = 1 mol m^{-3}, and δ_{EL} = 1 μm. It can be found that decreasing the pore diameter leads to an increase in the H_2O_2 production rate, but this again reaches a limit. Figure 2g shows that the mean oxygen concentration can reach a higher level as the pore diameter decreases (the cases d_{pore} = 300, 100, and 10 nm are 1.35, 1.48, and 1.55 times higher than the case d_{pore} = 1000 nm, respectively) and the oxygen concentration distribution becomes more uniform. Meanwhile, a smaller pore diameter means a thinner pore wall (in the case of d_{pore} = 1000, 300, 100, and 10 nm, δ_{wall} = 1500, 450, 150, and 15 nm). This reduces the diffusion distance of oxygen within the EL near the pore wall, and the EL in this region can obtain oxygen faster, thus increasing the oxygen supply rate (see Figure 2f) and H_2O_2 production rate. Figure 2h shows that as the pore diameter decreases, the difference in oxygen concentration between the two cutlines within the EL decreases, implying that oxygen concentration in the y direction becomes more uniform. When d_{pore} = 10 nm, the oxygen concentration level nearly reaches the level when gas is completely in contact with liquid, and the difference in oxygen concentration between two cutlines almost disappears. This implies that the smaller the pore diameter, the EL near the pore wall can obtain oxygen faster, resulting in a higher H_2O_2 production rate.

Effect of the Enzyme Layer Thickness. Figure 3a shows the effect of the EL thickness on the H_2O_2 production rate. The EL thicknesses range from 0.1 to 5 μm. The other parameters are d_{pore} = 100 nm, $[E_T]$ = 1 mol m^{-3}, and ϵ = 0.4. It can be found that increasing the EL thickness increases the H_2O_2 production rate, but this has a limit. As shown in Figure 3b, despite some differences in the oxygen concentration for the cases with different EL thicknesses, the oxygen concentration at the three-phase interface remains high. Increasing the EL thickness increases the reaction volume and oxygen consumption. However, this only slightly affects the oxygen concentration at the three-phase interface. Figure 3c shows that when the EL thickness is small, there is an excess of oxygen in the EL. Increasing the EL thickness enables excess oxygen to participate in the reaction (see Figure 3a) as a result, the H_2O_2 production rate increases. However, increasing the EL thickness simultaneously increases the diffusion distance of oxygen. This implies that diffusion struggles to meet reaction demand when the EL thickness is large, and most of the EL away from the three-phase interface are deprived of oxygen.

Effect of the Enzyme Concentration. Figure 3d shows the effect of the enzyme concentration on the H_2O_2 production rate. The enzyme concentrations range from 0.001 to 1000 mol m^{-3}. The other parameters are d_{pore} = 100 nm, δ_{EL} = 1 μm, and ϵ = 0.4. It can be found that increasing the enzyme concentration increases the H_2O_2 production rate, but it gradually reaches a plateau. Figure 3e shows that the reaction consumes more oxygen as the enzyme concentration increases, and the mean oxygen concentration at the three-phase interface decreases. Increasing the enzyme

https://doi.org/10.1021/acs.iecr.2c04492
Ind. Eng. Chem. Res. 2023, 62, 4337−4343

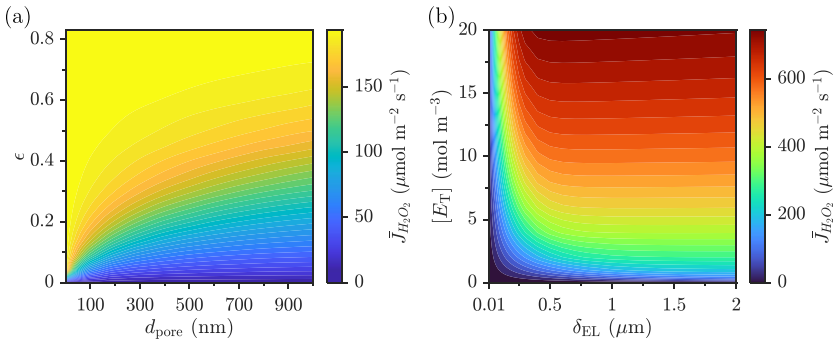

Figure 4. Effect of multiple parameters on the three-phase enzymatic reaction system. (a) Effect of d_{pore} and ϵ on the H_2O_2 production rate when $[E_T] = 1$ mol m^{-3} and $\delta_{EL} = 1$ μm. (b) Effect of δ_{EL} and $[E_T]$ on the H_2O_2 production rate when $d_{pore} = 100$ nm and $\epsilon = 0.4$.

concentration accelerates the reaction rate and consumes more oxygen, leading to gradual hypoxia of the EL near the pore wall. Figure 3f shows that there is sufficient oxygen within the EL at low enzyme concentrations. Increasing the enzyme concentration can accelerate the reaction rate. This leads to excess oxygen participation in the reaction (see Figure 3d), resulting in an increased H_2O_2 production rate. At higher enzyme concentrations, however, increasing the enzyme concentration further results in a reaction rate much greater than the mass transfer rate of oxygen. As a result, the oxygen supply from the gas phase is insufficient to meet the reaction demand, and most of the regions within the EL are deprived of oxygen.

Effect of Multiple Parameters. After analyzing the effect of individual parameters, the joint effect of multiple parameters is analyzed further. Figure 4a shows the effect of pore diameter and porosity on H_2O_2 production rate for a fixed enzyme concentration and EL thickness. It can be found that, regardless of the pore diameter, the H_2O_2 production rate will remain constant at higher values after a certain value of porosity is reached (e.g., $\epsilon > 0.8$). The pore diameter and porosity corresponding to the region with higher H_2O_2 production rate are the optimal parameter selection range for the substrate.

Figure 4b shows the effect of EL thickness and enzyme concentration on the H_2O_2 production rate with fixed pore diameter and porosity. It can be found that as long as the enzyme concentration is not too low (e.g., $[E_T] > 5$ mol m^{-3}), the H_2O_2 production rate almost no longer varies with increasing EL thickness after the EL thickness reaches a certain value (e.g., $\delta_{EL} > 0.5$ μm), and it increases almost linearly with increasing enzyme concentration.

In cases where the substrate parameters (pore diameter and porosity) are determined, these results can be used to guide the specification of enzyme layer parameters (EL thickness and enzyme concentration). Similarly, for specific enzyme layer thickness and concentration, the results in Figure 4 can be adopted for the construction of appropriate substrate structures.

CONCLUSIONS

A steady-state isothermal 2D model was developed here to investigate the effect of the three-phase interfacial microenvironment on the performance of the three-phase enzymatic reaction system based on glucose oxidase. Four parameters of the three-phase interfacial microenvironment have been studied, including the porosity, the pore diameter, the EL thickness, and the enzyme concentration. The results suggest that more H_2O_2 can be generated by increasing porosity, EL thickness, and enzyme concentration or by decreasing pore diameter. However, the H_2O_2 production rate could reach a plateau as these parameters are increased or decreased to a certain level. The results also reveal that the oxygen supply rate is a key factor in controlling the H_2O_2 production rate. This model should be an effective and promising tool for the design of three-phase enzymatic reaction system of superior performance with applications in disease diagnosis and health monitoring.

ASSOCIATED CONTENT

Supporting Information

The Supporting Information is available free of charge at https://pubs.acs.org/doi/10.1021/acs.iecr.2c04492.

Experimental details, modeling methods, and experimental validations, diagram of the experimental setup, comparison of experimental and simulation results, oxygen concentration profile, model parameters, and experimental parameters for the experiment I and II (PDF)

AUTHOR INFORMATION

Corresponding Authors

Jie Xiao − *College of Chemistry, Chemical Engineering and Materials Science, Soochow University, Suzhou, Jiangsu Province 215123, P. R. China; School of Chemical and Environmental Engineering, Soochow University, Suzhou, Jiangsu Province 215123, P.R. China;* orcid.org/0000-0001-7842-7862; Email: jie.xiao@suda.edu.cn

Xinjian Feng − *College of Chemistry, Chemical Engineering and Materials Science, Soochow University, Suzhou, Jiangsu Province 215123, P. R. China;* orcid.org/0000-0002-3646-9199; Email: xjfeng@suda.edu.cn

Authors

Siyu Zou − *College of Chemistry, Chemical Engineering and Materials Science, Soochow University, Suzhou, Jiangsu Province 215123, P. R. China;* orcid.org/0000-0002-9152-9844

Dandan Wang − *College of Chemistry, Chemical Engineering and Materials Science, Soochow University, Suzhou, Jiangsu Province 215123, P. R. China*

Complete contact information is available at: https://pubs.acs.org/10.1021/acs.iecr.2c04492

https://doi.org/10.1021/acs.iecr.2c04492
Ind. Eng. Chem. Res. 2023, 62, 4337−4343

Notes

The authors declare no competing financial interest.

■ ACKNOWLEDGMENTS

This work was supported by the National Key R&D Program of China (2019YFA0709200), the National Natural Science Foundation of China (21988102), the Jiangsu Funding Program for Excellent Postdoctoral Talent, the Priority Academic Program Development of Jiangsu Higher Education Institutions (PAPD), and the Project of Scientific and Technologic Infrastructure of Suzhou (SZS201905). Jie Xiao acknowledges the support from the National Natural Science Foundation of China (21978184).

■ REFERENCES

(1) Ruff, A.; Szczesny, J.; Marković, N.; Conzuelo, F.; Zacarias, S.; Pereira, I. A. C.; Lubitz, W.; Schuhmann, W. A fully protected hydrogenase/polymer-based bioanode for high-performance hydrogen/glucose biofuel cells. *Nat. Commun.* **2018**, *9*, 3675.

(2) Riedel, M.; Höfs, S.; Ruff, A.; Schuhmann, W.; Lisdat, F. A tandem solar biofuel cell: Harnessing energy from light and biofuels. *Angew. Chem., Int. Ed.* **2021**, *60*, 2078−2083.

(3) Wang, J. Electrochemical glucose biosensors. *Chem. Rev.* **2008**, *108*, 814−825.

(4) Zhao, L.; Yang, J.; Gong, M.; Li, K.; Gu, J. Specific screening of prostate cancer individuals using an enzyme-assisted substrate sensing platform based on hierarchical MOFs with tunable mesopore size. *J. Am. Chem. Soc.* **2021**, *143*, 15145−15151.

(5) Ge, L.; Zhao, Y.-s.; Mo, T.; Li, J.-r.; Li, P. Immobilization of glucose oxidase in electrospun nanofibrous membranes for food preservation. *Food Control* **2012**, *26*, 188−193.

(6) Fu, L.-H.; Qi, C.; Lin, J.; Huang, P. Catalytic chemistry of glucose oxidase in cancer diagnosis and treatment. *Chem. Soc. Rev.* **2018**, *47*, 6454−6472.

(7) Gao, L.; Zhuang, J.; Nie, L.; Zhang, J.; Zhang, Y.; Gu, N.; Wang, T.; Feng, J.; Yang, D.; Perrett, S.; Yan, X. Intrinsic peroxidase-like activity of ferromagnetic nanoparticles. *Nat. Nanotechnol.* **2007**, *2*, 577−583.

(8) Lei, Y.; Sun, R.; Zhang, X.; Feng, X.; Jiang, L. Oxygen-rich enzyme biosensor based on superhydrophobic electrode. *Adv. Mater.* **2016**, *28*, 1477−1481.

(9) Chen, L.; Sheng, X.; Wang, D.; Liu, J.; Sun, R.; Jiang, L.; Feng, X. High-Performance Triphase Bio-Photoelectrochemical Assay System Based on Superhydrophobic Substrate-Supported TiO2 Nanowire Arrays. *Adv. Funct. Mater.* **2018**, *28*, 1801483.

(10) Wu, Y.; Feng, J.; Gao, H.; Feng, X.; Jiang, L. Superwettability-based interfacial chemical reactions. *Adv. Mater.* **2019**, *31*, 1800718.

(11) Sheng, X.; Liu, Z.; Zeng, R.; Chen, L.; Feng, X.; Jiang, L. Enhanced Photocatalytic Reaction at Air-Liquid-Solid Joint Interfaces. *J. Am. Chem. Soc.* **2017**, *139*, 12402−12405.

(12) Zhou, H.; Sheng, X.; Xiao, J.; Ding, Z.; Wang, D.; Zhang, X.; Liu, J.; Wu, R.; Feng, X.; Jiang, L. Increasing the efficiency of photocatalytic reactions via surface microenvironment engineering. *J. Am. Chem. Soc.* **2020**, *142*, 2738−2743.

(13) Jin, Z.; Wang, L.; Zuidema, E.; Mondal, K.; Zhang, M.; Zhang, J.; Wang, C.; Meng, X.; Yang, H.; Mesters, C.; Xiao, F.-S. Hydrophobic zeolite modification for in situ peroxide formation in methane oxidation to methanol. *Science* **2020**, *367*, 193−197.

(14) Mi, L.; Yu, J.; He, F.; Jiang, L.; Wu, Y.; Yang, L.; Han, X.; Li, Y.; Liu, A.; Wei, W.; Zhang, Y.; Tian, Y.; Liu, S.; Jiang, L. Boosting Gas Involved Reactions at Nanochannel Reactor with Joint Gas-Solid-Liquid Interfaces and Controlled Wettability. *J. Am. Chem. Soc.* **2017**, *139*, 10441−10446.

(15) Guan, F.; Zhang, J.; Tang, H.; Chen, L.; Feng, X. An enhanced enzymatic reaction using a triphase system based on superhydrophobic mesoporous nanowire arrays. *Nanoscale Horiz* **2019**, *4*, 231−235.

(16) Wang, H.; Zhang, J.; Wang, D.; Wang, Z.; Chen, Y.; Feng, X. Flexible triphase enzyme electrode based on hydrophobic porous PVDF membrane for high-performance bioassays. *Biosens. Bioelectron.* **2021**, *183*, 113201.

(17) Zha, J.; Zou, S.; Hao, J.; Liu, X.; Delaplace, G.; Jeantet, R.; Dupont, D.; Wu, P.; Dong Chen, X.; Xiao, J. The role of circular folds in mixing intensification in the small intestine: A numerical study. *Chem. Eng. Sci.* **2021**, *229*, 116079.

(18) Xiao, J.; Shen, Q.; Chen, X. D. Uncovering eco-friendly design in the ancient bronze goose-and-fish lamp: An unnoticeable gap boosts ventilation. *PNAS* **2022**, *119*, No. e2202037119.

(19) Parker, J. W.; Schwartz, C. S. Modeling the kinetics of immobilized glucose oxidase. *Biotechnol. Bioeng.* **1987**, *30*, 724−735.

(20) Gao, M.; Hazelbaker, M. S.; Kong, R.; Orazem, M. E. Mathematical model for the electrochemical impedance response of a continuous glucose monitor. *Electrochim. Acta* **2018**, *275*, 119−132.

(21) Weng, L.-C.; Bell, A. T.; Weber, A. Z. Modeling gas-diffusion electrodes for CO2 reduction. *Phys. Chem. Chem. Phys.* **2018**, *20*, 16973−16984.

(22) Baronas, R.; Ivanauskas, F.; Kulys, J. Effects of diffusion limitations on the response and sensitivity of biosensors. *Mathematical Modeling of Biosensors: An Introduction for Chemists and Mathematicians*, 2nd ed.; Springer: Cham, 2021; pp 49−84.

(23) Blake, J. W.; Padding, J. T.; Haverkort, J. W. Analytical modelling of CO2 reduction in gas-diffusion electrode catalyst layers. *Electrochim. Acta* **2021**, *393*, 138987.

(24) Yang, Z.; Li, D.; Xing, L.; Xiang, H.; Xuan, J.; Cheng, S.; Yu, E. H.; Yang, A. Modeling and upscaling analysis of gas diffusion electrode-based electrochemical carbon dioxide reduction systems. *ACS Sustainable Chem. Eng.* **2021**, *9*, 351−361.

(25) Lees, E. W.; Bui, J. C.; Song, D.; Weber, A. Z.; Berlinguette, C. P. Continuum model to define the chemistry and mass transfer in a bicarbonate electrolyzer. *ACS Energy Lett.* **2022**, *7*, 834−842.

(26) Bird, R. B.; Stewart, W. E.; Lightfoot, E. N. Diffusivity and the mechanisms of mass transport. *Transport Phenomena*, 2nd ed.; John Wiley & Sons: New York, 2002; pp 513−542.

(27) Chen, X.-M.; Xiao, J.; Zhu, Y.-P.; Luo, Z.-H. Intraparticle mass and heat transfer modeling of methanol to olefins process on SAPO-34: A single particle model. *Ind. Eng. Chem. Res.* **2013**, *52*, 3693−3707.

(28) Poling, B. E.; Prausnitz, J. M.; O'connell, J. P. Diffusion coefficients. *The Properties of Gases and Liquids*, 5th ed.; Mcgraw-Hill: New York, 2001; pp 635−689.

(29) Tao, Z.; Raffel, R. A.; Souid, A.-K.; Goodisman, J. Kinetic studies on enzyme-catalyzed reactions: Oxidation of glucose, decomposition of hydrogen peroxide and their combination. *Biophys. J.* **2009**, *96*, 2977−2988.

(30) Atkinson, B.; Lester, D. E. An enzyme rate equation for the overall rate of reaction of gel-immobilized glucose oxidase particles under buffered conditions. I. Pseudo-one substrate conditions. *Biotechnol. Bioeng.* **1974**, *16*, 1299−1320.

(31) Atkinson, B.; Lester, D. E. An enzyme rate equation for the overall rate of reaction of gel-immobilized glucose oxidase particles under buffered conditions. II. Two limiting substrates. *Biotechnol. Bioeng.* **1974**, *16*, 1321−1343.

(32) Gros, P.; Bergel, A. Improved model of a polypyrrole glucose oxidase modified electrode. *J. Electroanal. Chem.* **1995**, *386*, 65−73.

https://doi.org/10.1021/acs.iecr.2c04492
Ind. Eng. Chem. Res. 2023, 62, 4337−4343